

Density Functional Theory Study of the Adsorption of Alkanethiols on Cu(111), Ag(111), and Au(111) in the Low and High Coverage Regimes

F. P. Cometto,[†] P. Paredes-Olivera,[†] V. A. Macagno,[‡] and E. M. Patrito^{*,‡}

Unidad de Matemática y Física and Departamento de Fisicoquímica, Instituto de Investigaciones en Fisicoquímica de Córdoba (INFIQC), Facultad de Ciencias Químicas, Universidad Nacional de Córdoba, Ciudad Universitaria, 5000 Córdoba, Argentina

Received: June 17, 2005; In Final Form: September 19, 2005

The structure, the surface bonding, and the energetics of alkanethiols adsorbed on Cu(111), Ag(111), and Au(111) surfaces were studied under low and high coverages. The potential energy surfaces (PES) for the thiol/metal interaction were investigated in the absence and presence of externally applied electric fields in order to simulate the effect of the electrode potential on the surface bonding. The electric field affects the corrugation of the PES which decreases for negative fields and increases for positive fields. In the structural investigation, we considered the relaxation of the adsorbate and the surface. The highest relaxation in a direction perpendicular to the surface was observed for gold atoms, whereas silver atoms presented the highest relaxation in a plane parallel to the surface. The surface relaxation is more important in the low coverage limit. The surface bonding was investigated by means of the total and projected density of states analysis. The highest ionic character was observed on the copper surface whereas the highest covalent character occurs on gold. This leads to a strong dependence of the PES with the tilt angle of the adsorbate on Au(111) whereas this dependence is less pronounced on the other metals. Thus, the adsorbate-relaxation and the metal-relaxation contributions to the binding energy are more important on gold. The adsorption of thiols on gold was investigated on the 111 surface as well as on a surface with gold adatoms in order to elucidate the effect of thiols on the surface diffusion of gold. The $\text{CH}_3\text{CH}_2\text{S}$ radical adsorbs on top of the gold adatom. The diffusional barrier of the $\text{CH}_3\text{CH}_2\text{SAu}$ species is lower than that for a bare gold adatom and is also lower than that for the bare thiol radical. The adsorption of the molecular species CH_3SH and $\text{CH}_3\text{CH}_2\text{SH}$ was also investigated on Au(111). They adsorb via the sulfur atom on top of a gold atom. On the other hand, the adsorption of the alkanethiol radicals on the perfect 111 surfaces occurs on the face centered cubic (fcc)-bridge site in the low coverage limit for all metals and shifts toward the fcc site at high coverage on copper and silver.

Introduction

The characterization of the potential energy surface of alkanethiols on coinage metals is a key issue in order to understand the many physical and chemical transformations that take place from the formation to the desorption of a self-assembled monolayer, such as lifting or induction of substrate reconstruction processes, formation of different rotational domains and superstructures, increased surface mobility at the onset of reductive desorption under electrochemical conditions, etc.

The calculation of the potential energy surface for alkanethiols is a difficult task because it depends on a large number of variables. In the low coverage limit, we can identify variables that depend on the molecular backbone and on the position of the sulfur atom above the surface. The orientation of the molecular back-bond on the surface is described by three angles: the tilt of the molecular axis with respect to surface normal, the tilt direction, and the twist angle (which corresponds to a rotation about the molecular axis). Under conditions of high coverage, chain–chain interactions as well as interac-

tions between end groups add new variables to the potential energy surface. The sulfur–metal interaction (which is a function of the surface coverage) weakens the interaction among the metal atoms of the first layers which, thus, may undergo a surface reconstruction process. Therefore, the complexity of the alkanethiol–metal system shows that the knowledge of the potential energy surface is far from complete from a first principles point of view and is certainly crucial for future developments and application of self-assembled monolayers (SAMs).

The $\text{CH}_3\text{S}/\text{Au}(111)$ system has been the most studied using different quantum mechanical methods.^{1–12} It is well established that the most stable binding site lies in the vicinity of the bridge site with both the face centered cubic (fcc)-bridge and hexagonal close packed (hcp)-bridge sites being almost equally stable. Potential energy surfaces have been mainly studied for methanethiol under high coverage conditions as a function of the surface displacement along the top-fcc-bridge-hcp line and the tilt of the S–C bond with the surface normal.⁷ The potential energy surfaces of longer chain thiols such as propanethiol were investigated keeping the molecular plane perpendicular to the surface.¹¹

The adsorption of alkanethiols on Cu and Ag has been less studied than on Au. The influence of relativistic effects on the methanethiolate chemisorption bond was pointed out by Sellers

* To whom correspondence should be addressed. E-mail: martin@fcq.unc.edu.ar. Tel: 54-351-4334169/54-351-4334180. Fax: 54-351-4334188.

[†] Unidad de Matemática y Física.

[‡] Departamento de Fisicoquímica.

et al.¹ for the Au(111) and Ag(111) surfaces and was also studied on the 111 faces of Cu, Ag, and Au.⁵ We recently investigated the chemisorption of alkanethiols on Cu(111) as a function of the chain length and chain orientation at the MP2 level of theory.¹³ We found a weak dependence of the binding energy with the tilting of the alkyl chain which was consistent with the ionic nature of the bonding. On the Ag(111) surface, we comparatively studied the adsorption of the canonical thiourea and methanethiolate radicals, (NH₂)(NH)CS• and CH₃S•, to elucidate the influence of the amino terminal groups on the surface bonding.¹⁴ The theoretical studies of alkanethiolate adsorption on Cu and Ag reported in the literature correspond to the low coverage limit as they were performed using the cluster model of the surface. Investigations under high coverage conditions have not been reported yet.

In this paper, we performed a comparative investigation of the structure and energetics of *n*-alkanethiols on the Cu(111), Ag(111), and Au(111) surfaces under low and high coverages. The potential energy surfaces of the alkanethiol–metal system were investigated in the absence and presence of external electric fields in relation to the processes of formation as well as reductive desorption of SAMs. The electric field has an important effect on the corrugation of the potential energy surface. The extent of adsorbate-induced surface relaxation was investigated under low and high coverages. On the gold surface, we also considered the adsorption of the methanethiol and ethanethiol molecular species. Whereas the molecules adsorb via the sulfur atom on ontop sites, the corresponding radicals adsorb close to a bridge site on the perfect surfaces. However, in the presence of surface adatoms, the radical species adsorb ontop of the adatom and decrease its barrier for surface diffusion.

Surface Modeling and Theoretical Methods

The adsorption on the 111 surfaces in the low coverage regime was modeled using a metal cluster with 25 metal atoms distributed in two layers (16 atoms in the first layer and 9 in the second layer). The advantage of the cluster approach is that it allows the electric field at an electrochemical interface to be modeled by applying external electric fields perpendicular to the cluster surface. Kohn–Sham one-electron equations were solved using the Vosko–Wilk–Nusair (VWN) functional¹⁵ to obtain the local potential. Gradient corrections for the exchange (Becke functional¹⁶) and correlation (Perdew functional¹⁷) energy terms were self-consistently included. The binding energy of the methanethiolate radical calculated with the BP86 functional^{16,17} was also compared with the binding energies obtained using the BLYP^{16,18} and PW91¹⁹ functionals. We observed a very good agreement between the different functionals giving adsorbate binding energies which did not differ by more than 2 kcal/mol. We used a triple- ζ basis set with one set of polarization functions for both the metal atoms and the S, C, and H atoms of the adsorbates. Slater type orbitals were used as basis sets. The frozen core approximation was employed to describe the innermost atomic shells of the metal atoms. The frozen core orbitals included up to the 3p, 4p, and 4f orbitals for Cu, Ag, and Au, respectively. Relativistic effects were taken into account using the zero-order regular approximation (ZORA).²⁰ The Amsterdam density functional program (ADF)²¹ was used in these calculations modeling the low coverage regime.

The periodic supercell approach was employed to describe the ($\sqrt{3} \times \sqrt{3}$)R30° structure of methanethiolate on Cu(111), Ag(111), and Au(111). The surface was represented by a slab with four layers of metal atoms. The positions of all the atoms

in the unit cell (except the metal atoms in the fourth layer) were relaxed in the potential energy determined by the full quantum mechanical electronic structure. The convergence criterion for geometry optimizations was a RMS force of 0.01 eV/Å. A vacuum thickness of 18 Å was introduced between the thiolated slabs to avoid spurious interactions between neighboring replicas. Only one side of the metal slab was covered by thiols. The first principle atomistic calculations were performed using state-of-the-art plane-wave periodic DFT.²² Gradient corrections were included in the exchange correlation functional in the PBE formulation.²³ Ultrasoft²⁴ pseudopotentials were used for the atomic species taking into account scalar relativistic effects for Ag, Au, and S atoms. The electron wave functions were expanded in a plane-wave basis set up to a kinetic energy cutoff of 22 Ry (180 Ry for the density). Brillouin zone integration was performed using a (6 × 6 × 1) Monkst–Pack mesh.²⁵ To ensure that there are not residual forces in the unit cell, we determined the equilibrium bulk structure for Cu, Ag, and Au obtaining the following values for a_0 : 3.6820, 4.1730, and 4.1768 Å, respectively. Our calculated bulk modulus values are 144.5, 102.2, and 154.9 GPa for Cu, Ag, and Au.

In the cluster calculations, binding energies were obtained by subtracting the total energy of the bare metal cluster and the bare adsorbate from the cluster–adsorbate composite energy

$$BE = E_{\text{adsorbate-cluster}} - E_{\text{adsorbate}} - E_{\text{cluster}} \quad (1)$$

In the periodic calculations, the binding energies were calculated in the same manner. In this case, we considered the energies of the adsorbate–slab unit cell, bare slab unit cell, and free adsorbate. Negative values of binding energies indicate a stabilization of the substrate–adsorbate system with respect to the bare adsorbate and bare metal.

Results and Discussion

Potential Energy Surfaces of CH₃S in the Low Coverage Limit. In this section, we first consider the potential energy surfaces for methanethiolate adsorption as a function of the position of the sulfur atom on the surface and the tilt of the S–C bond with respect to the surface normal as schematized in Figure 1. The sulfur atom of methanethiol was displaced at a constant height above the surface from the fcc toward the hcp-hollow sites. The height of the sulfur atom above the surface shows a very small dependence on the tilt angle and the surface site position along the fcc-bridge-hcp path. We used the following values: 1.905 Å on Cu(111), 2.110 Å on Ag(111), and 1.985 Å on Au(111). All the calculations were performed with the methyl group in a staggered position with respect to the three metal atoms defining the hollow site. In this configuration, the hydrogen atoms point toward the bridge sites (see top views in Figure 1). Therefore, when passing through the bridge site, the methyl group was rotated 60° to keep the staggered configuration as shown in Figure 1. The staggered and eclipsed configurations have the same energy at the bridge site when the S–C bond is perpendicular to the surface (zero tilt). The eclipsed configuration becomes less stable than the staggered configuration as the tilt increases, although the difference is small. At the equilibrium tilt angle (around 60°), for example, the binding energy of CH₃S on Au(111) is −41.4 kcal/mol for the eclipsed configuration whereas it is −42.4 kcal/mol for the staggered configuration.

Figure 2 shows the potential energy surfaces (PESs) on the three metal surfaces. The PES has two minima on either side of the bridge site and a maximum exactly on the bridge site for

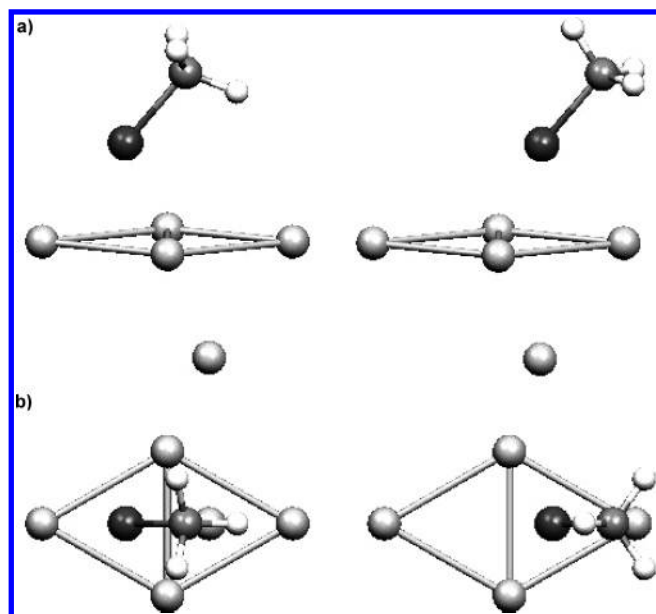


Figure 1. (a) Side and (b) top views showing the surface displacement of CH₃S from the fcc to the hcp-hollow sites. The hydrogen atoms of the methyl group are in a staggered orientation with respect to the three metal atoms that define the hollow site.

a tilt angle of zero degrees. The magnitude of the tilt angles in the minima are between 50° and 60°, being larger on the gold surface. The positive tilt angles around the minimum located in the fcc-bridge position (see Figure 1) as well as the negative tilt angles around the hcp-bridge position indicate that the S–C bond is tilted toward the bridge site. The magnitude and location of the critical points of the PES are summarized in Table 1. The binding energy of methanethiolate is higher on the fcc-bridge site than that on the hcp-bridge site. However, the difference is less than 1 kcal/mol. Although both minima are nearly isoenergetic, the diffusion of methanethiolate from one site to the other implies the passage through the bridge site with a zero tilt. This configuration is several kcal/mol less stable as shown in Table 1. The energy difference between the minimum in the fcc-bridge position and the maximum in the bridge position gives the corrugation of the PES with respect to the tilt angle. With the data in Table 1, we obtained 9.47, 7.85, and 17.60 kcal/mol on the Cu, Ag, and Au surfaces, respectively. Although the highest binding energies are obtained on the more reactive copper surface, the highest corrugation is observed on gold. The last columns of Table 1 show that on the fcc site the minima are located closer to the bridge site than to the hcp site. In the case of copper and silver, the Δ_{bridge} values of 0.40 and 0.43 Å indicate that the hcp-bridge minimum is located in an intermediate position between the bridge and the hcp site.

When methanethiolate adsorbs with zero tilt (S–C bond perpendicular to the surface), we observe that the ordering of binding energies is Cu > Ag > Au on the bridge and ontop sites (Table 1). The same ordering is obtained on the hollow-hcp and hollow-fcc sites for zero tilt as shown in Table 2. At zero tilt, the adsorption of methanethiolate on copper is more stable than that on gold by 13.97 kcal/mol (bridge site), 18.05 kcal/mol (top site), 11.42 kcal/mol (fcc-hollow site), and 13.10 kcal/mol (hcp-hollow site). However, the energy difference between the binding energies on copper and gold is lower at the equilibrium tilt angle. The binding energy on Cu is only 5.8 kcal/mol more stable than that on gold on the fcc-bridge and hcp-bridge sites (see Table 1). This indicates that the adsorption of methanethiolate on gold is much more stabilized

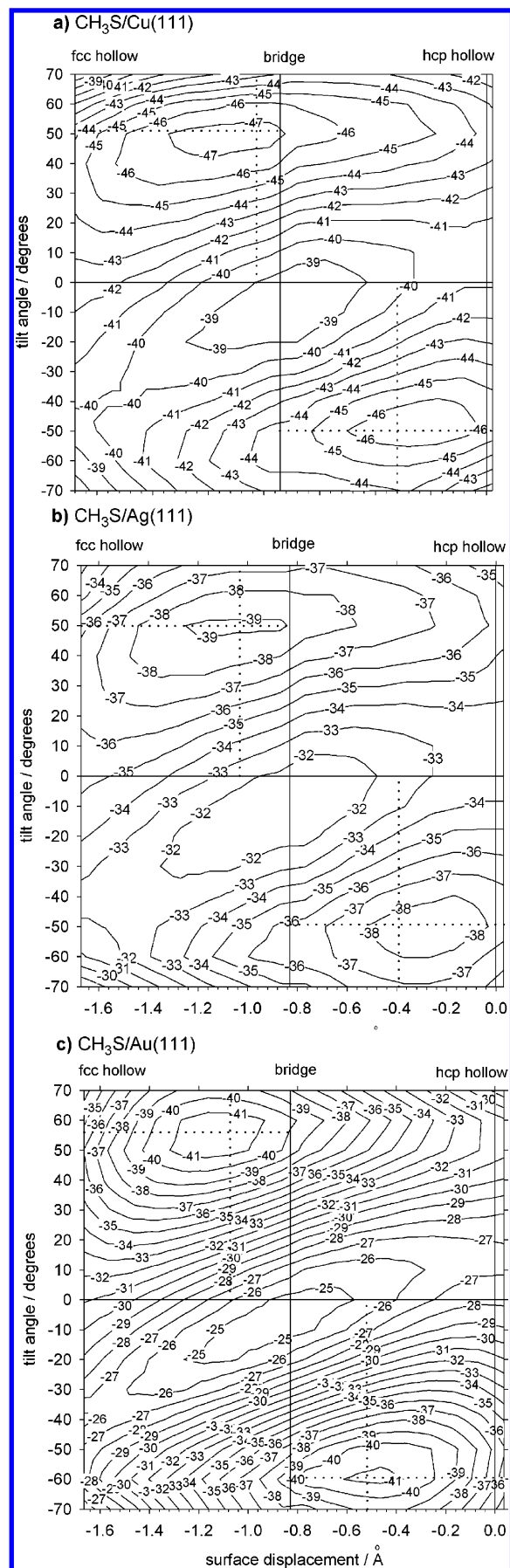


Figure 2. Potential energy surfaces of CH₃S on (a) Cu(111), (b) Ag(111), and (c) Au(111) as a function of the tilt angle of the S–C bond with respect to the surface normal and the surface displacement of the sulfur atom along the fcc-bridge-hcp path.

TABLE 1: Magnitude and Location of Critical Points in the Potential Energy Surface^a

	BE/kcal/mol			tilt/deg			Δ bridge/Å		
	Cu	Ag	Au	Cu	Ag	Au	Cu	Ag	Au
fcc-brd	-48.20	-39.58	-42.36	52.1	49.8	56.4	0.11	0.27	0.25
hcp-brd	-47.40	-39.20	-41.55	-50.1	-49.0	-59.5	0.40	0.43	0.31
bridge	-38.73	-31.73	-24.76	0.0	0.0	0.0			
ontop	-30.60	-23.46	-12.55	0.0	0.0	0.0			

^a Minima are found on the fcc-bridge and hcp-bridge sites. Maxima are found on the bridge and ontop sites at zero tilt.

TABLE 2: Binding Energy of CH₃S Adsorbed on the fcc- and hcp-Hollow Sites with the S–C Bond Perpendicular to the Surface

	BE/kcal/mol		
	Cu	Ag	Au
fcc, $\theta = 0^\circ$	-42.55	-35.31	-31.13
hcp, $\theta = 0^\circ$	-40.91	-33.55	-27.81

by the tilting of the S–C bond than on the silver and copper surfaces. The binding energies on the fcc-bridge and hcp-bridge sites have the following order at the equilibrium tilt: Cu > Au > Ag (Table 1). The binding energy of -48.2 kcal/mol obtained on the unrelaxed Cu(111) surface compares very well with the binding energy of -47.0 kcal/mol that we obtained in a previous study¹³ at the HF + MP2 level of theory.

To evidence more clearly the sensitivity of the PES with respect to the tilt angle, the binding energy of methanethiolate along the fcc-bridge-hcp path was plotted for the equilibrium and zero tilt angles (Figure 3). On all the metals, the maximum deviation of both curves is observed around the bridge site. On the Cu and Ag surfaces, the curves are flatter and closer to each other than those on the Au surface. This behavior clearly shows the higher directionality of the surface bonding on gold which is due to a higher covalent nature as we will discuss in the next section. In Figure 3c, we also included the PES of the HS• radical. At zero tilt (S–H bond perpendicular to the surface), the PES virtually coincides with that of the CH₃S• radical. However, at the equilibrium tilt of 80°, HS• has a higher binding energy than CH₃S• and the minimum energy is obtained on the bridge site instead of the fcc-bridge site as is the case for CH₃S•. The fact that the binding energies of HS• and CH₃S• differ at the equilibrium tilt whereas they are the same on all surface sites when the S–H and S–CH₃ bonds are perpendicular to the surface indicates that the sulfur–methyl back-bond of methanethiolate is involved in a larger steric repulsion with the surface than the sulfur–hydrogen back-bond of mercapto. For the sake of comparison, we also plotted in Figure 3d the PES of a single sulfur atom. In this case, the hollow sites are the most stable with binding energies which are roughly two times higher than the binding energies of HS• and CH₃S•.

The strong dependence of the PES on the tilt angle on gold was also observed on the ontop site, as shown in Figure 4. The PES on this site has a higher corrugation on Au than on Ag and Cu. The curves have two minima around $\pm 60^\circ$ corresponding to a tilt toward the hcp or the fcc sites. Unlike other high-symmetry sites, the energy ordering of methanethiolate binding energies on the ontop site is Cu > Ag > Au for all tilt angles. In all these calculations, the plane that contains the C, S, and one of the H atoms of CH₃S was kept normal to the surface. If this plane is tilted with respect to the surface normal, the potential energy on the fcc-bridge and hcp-bridge sites increases. This indicates that these sites are also minima with respect to the tilting of the molecular plane. However, this is not the case for longer alkyl chains, as will be shown below.

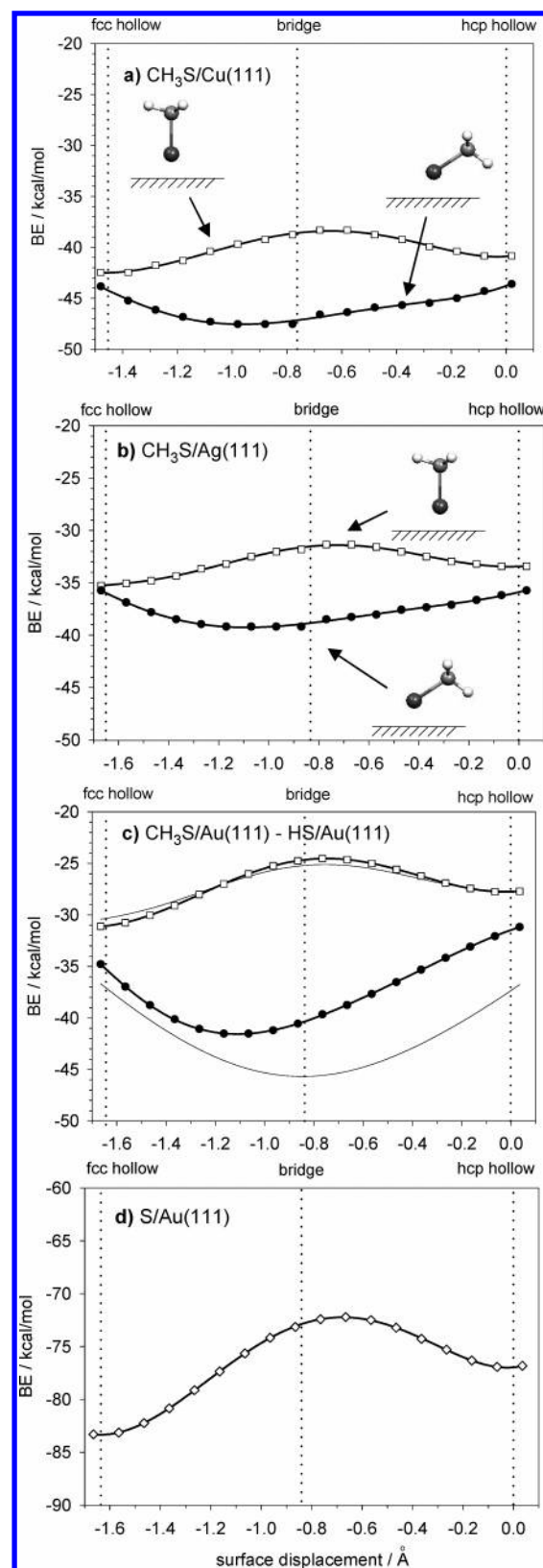


Figure 3. Binding energy of CH₃S along the fcc-bridge-hcp path for zero tilt (open squares) and equilibrium tilt (filled circles) on (a) Cu(111), (b) Ag(111), and (c) Au(111). The solid lines in graph c correspond to the binding energy of HS at zero tilt (upper curve) and the equilibrium tilt of 80° (lower curve). (d) Binding energy of sulfur atom on Au(111) along the fcc-bridge-hcp path.

Surface Bonding. To rationalize the observed trends in binding energies and, particularly, the important effect of the tilt angle on the gold surface, we investigated in this section

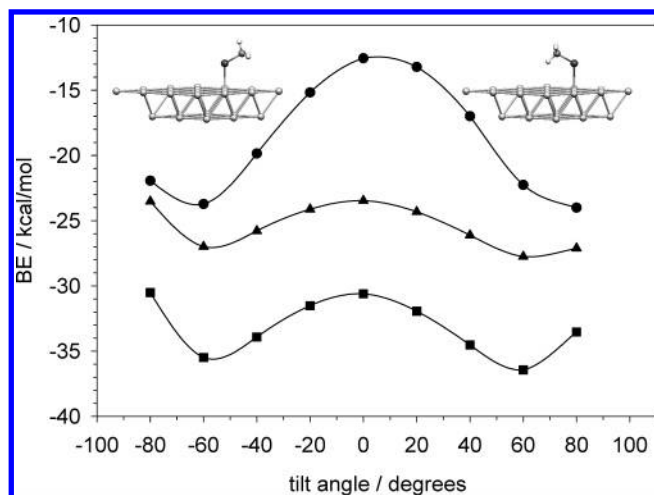


Figure 4. Binding energy of CH_3S as a function of tilt angle calculated on the ontop site of Cu(111), Ag(111), and Au(111). The highest corrugation is observed on the Au(111) surface.

the main features of the surface bonding on the three metals. The partial density of states (PDOS) of the S(3p) orbitals and the crystal orbital overlap population (COOP) between the S(3p) and the metal (M) d and sp bands were used to characterize the surface bonding. The COOP gives the (anti-) bonding character of the states in the PDOS: the COOP has large positive values at energies where the interaction between two orbitals is bonding and negative values where the interaction is antibonding.²⁶

The valence molecular orbitals of the methanethiolate radical and their energies are σ (−19.3 eV), σ^* (−15.6 eV), π (−11.0 eV), π (−10.7 eV), σ (−9.0 eV), π^* (−6.2 eV), and π^* (−5.6 eV). The energy levels (artificially broadened) are shown in Figure 5a as a density of states (DOS) plot. The two σ orbitals at the lowest energies arise from the overlap of the 2s and 3p_z (oriented along the S–C bond) atomic orbitals of C and S and the 1s orbitals of H. The two bonding π orbitals have a major contribution from the C(2p_{xy}) orbitals, while the two antibonding π^* orbitals have a major contribution from the S(3p_{xy}) orbitals. The d and sp bands of all the metals are located at higher energies than those of the two first σ orbitals. Therefore, the dispersion of these states upon adsorption is very small as can be observed in the S(3p) projected DOS of parts b and c of Figure 5 on all the metals. The COOP curves show that the S(3p)/M(d) and the S(3p)/M(sp) interaction of the S(3p) orbitals involved in the σ^* MO of methanethiol is bonding (peaks at energies −16.5, −15.1, and −15.7 eV on Au, Ag, and Cu). This is a clear example of an electrostatic interaction between bands separated in energy. This interaction increases in the order Au, Ag, and Cu indicating that the most ionic bonding occurs on the copper surface.

On the other hand, the DOS of the remaining π , π , σ , π^* , and π^* states of methanethiol overlaps with the DOS of the d and sp bands giving rise to different bonding and antibonding covalent interactions as observed in the COOP plots. In the case of gold, the S(3p)/Au(5d) and S(3p)/Au(6sp) interactions are antibonding close to the Fermi energy with some bonding interactions at lower energies. The reverse trend is observed on the copper surface: the COOP curves indicating antibonding states close to the Fermi energy are lower in magnitude whereas the bonding interactions at lower energies are higher. This indicates that covalent interactions on copper are less important than those on gold. The interaction with the metal sp band is mostly antibonding on gold whereas on silver it has an important

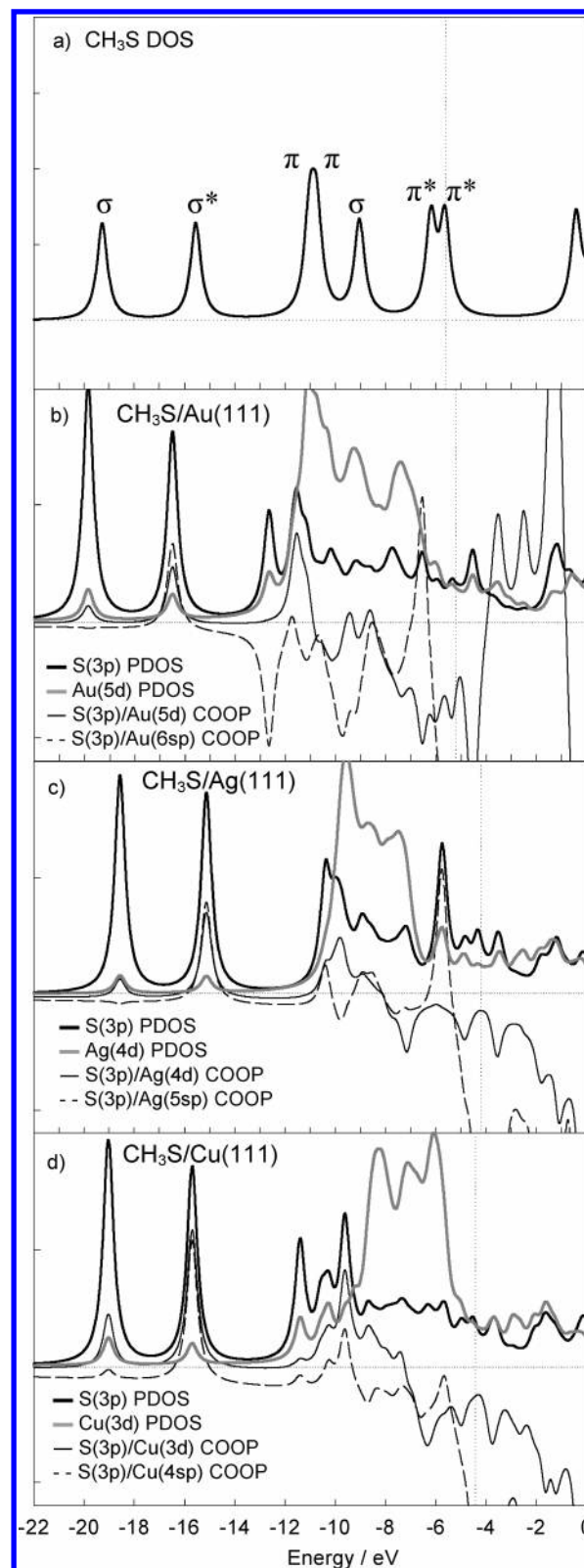


Figure 5. (a) Total DOS of the free CH_3S radical. Projected DOS and COOP curves on (b) Au(111), (c) Ag(111), and (d) Cu(111): thick solid line, PDOS of S(3p) orbitals; thick gray line, PDOS of metal d orbitals; thin solid line, COOP for the S(3p)/M(d) interaction; thin dashed line, COOP for the S(3p)/M(sp). The vertical dashed line in b–d indicates the Fermi energy.

bonding peak at −5.7 eV. From Figure 5d, it becomes clear that copper is the most reactive surface as it has more bonding and less antibonding interactions with the methanethiol orbitals than on the other surfaces.

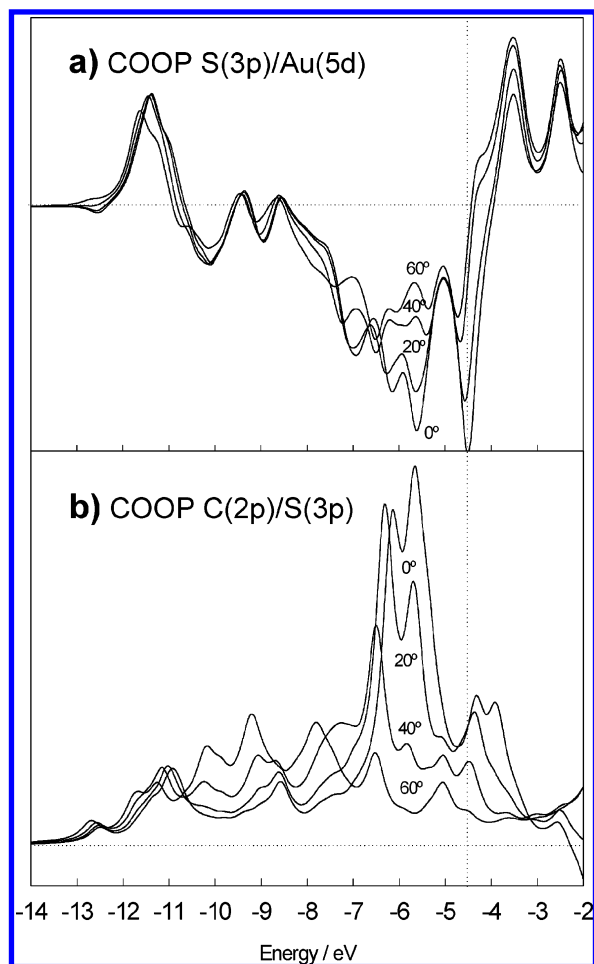


Figure 6. (a) S(3p)/Au(5d) and (b) C(2p)/S(3p) COOP curves for CH₃S/Au(111) as a function of the tilt of the S–C bond with respect to the surface normal for adsorption on the fcc-bridge site. The vertical dashed line indicates the Fermi energy.

From the previous analysis, we can now rationalize the sensitivity of the PES with respect to the tilt angle of methanethiol on the gold surface. In Figure 6a, we plotted the COOP curves for the S(3p)/Au(5d) interaction at various tilt angles. The tilt mainly affects the COOP curves at energies close to the Fermi energy where the interaction is antibonding. As the tilt of the S–C bond decreases (the methanethiolate radical becomes perpendicular to the surface), the S(3p)/Au(5d) interaction becomes more antibonding. Figure 6b shows the COOP curves for the interaction between the 2p orbitals of C and the 3p orbitals of S atoms of methanethiol. It is observed that this interaction strengthens as the tilt decreases. This is a clear example of the conservation of bond order²⁷ on metal surfaces: as the S(3p)/Au(5d) interaction weakens with decreasing tilt angles, the C(2p)/S(3p) interaction strengthens.

The high sensitivity of the PES with the tilt angle (fcc-bridge or ontop sites) implies that SAMs on gold will have rotational domains with disordered regions in the domain boundaries because the interconversion among the different domains requires high energies. Disordered regions can be envisaged from the collapse of domains with positive and negative tilts oriented along the different symmetry directions of the Au(111) surface. This points out the importance of annealing SAMs on gold to obtain more compact monolayers. In another section, we will show that the electrode potential (due to its effect on the PES) in oxidative adsorption experiments is another tool that may provide control on the growth and compactness of SAMs.

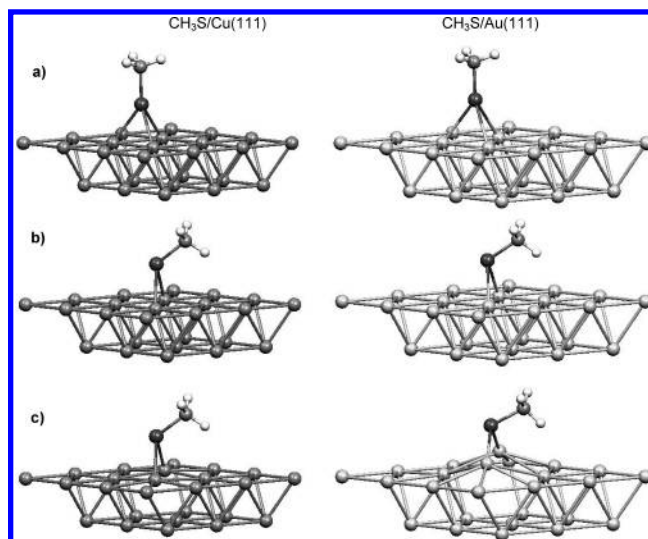


Figure 7. Equilibrium structures of CH₃S on Cu(111) (left) and Au(111) (right) for (a) adsorption on the fcc-hollow site at zero tilt, (b) relaxed adsorbate on the fixed metal surface, and (c) relaxed adsorbate and relaxed metal atoms in the primary adsorption site.

TABLE 3: Contributions to the Binding Energy (in kcal/mol) from the Adsorbate and Metal Relaxation^a

	Cu		Ag		Au	
	BE	ΔBE	BE	ΔBE	BE	ΔBE
unrelaxed adsorbate	−42.55		−35.31		−31.13	
(fcc) unrelaxed metal						
relaxed adsorbate	−48.20	−5.66	−39.58	−4.27	−42.36	−11.23
unrelaxed metal						
relaxed adsorbate	−50.57	−2.37	−43.26	−3.68	−52.99	−10.63
relaxed metal						

^a The initial geometry corresponds to CH₃S adsorbed on the fcc-hollow site with the S–C bond perpendicular to the surface.

Surface Relaxation in the Low Coverage Limit. In this section, we consider the effect of the relaxation of the atoms in the primary chemisorption site on the structure and energetics of methanethiolate adsorption. We performed a set of geometry optimizations starting with CH₃S adsorbed with zero tilt at the equilibrium surface distance on the fcc hollow site (Figure 7a). When the coordinates of the adsorbate were relaxed, it tilted and moved to the fcc-bridge site (Figure 7b). In the last step, the coordinates of the three atoms of the hollow site (together with those of the adsorbate) were allowed to relax until the energy minimum was found. The metal relaxation is considerably larger on gold than on the other two metals (compare Figure 7c on Cu and Au). Table 3 contains the binding energies on the three metals for the sequence of steps shown in Figure 7. The relaxation of the adsorbate, keeping the metal atoms fixed, contributes −5.66, −4.27, and −11.23 kcal/mol to the binding energy on Cu, Ag, and Au. In the last step, the metal relaxation contributes −2.37, −3.68, and −10.63 to the binding energy on Cu, Ag, and Au, respectively. These data show the unique behavior of methanethiolate on the Au(111) surface: the adsorbate-relaxation and metal-relaxation contributions to the binding energy are between two and three times higher than those on the other metals. When the metal relaxation is taken into account, we arrive at the surprising result that the ordering of binding energies in the low coverage limit is Au > Cu > Ag.

Table 4 compares different geometric parameters for the relaxed and unrelaxed metal substrates. The adsorbate mainly induces an upward relaxation of the two metal atoms which

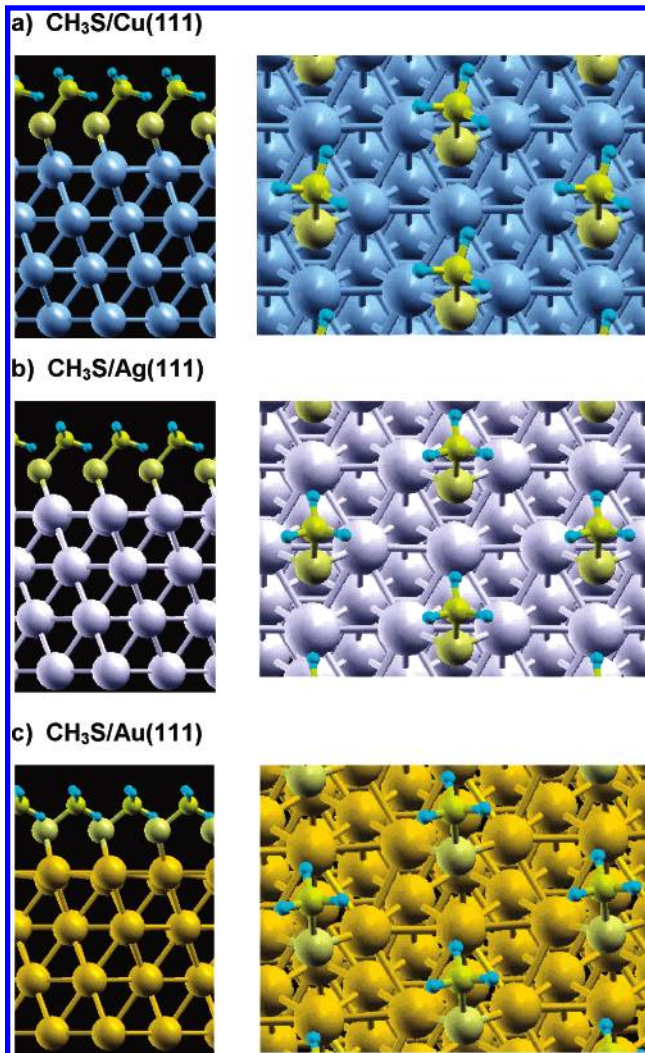
TABLE 4: Comparison of Geometrical Parameters for the Equilibrium Geometry of CH₃S Adsorbed on the Relaxed and Unrelaxed Metal Surfaces

	Cu		Ag		Au	
	relaxed	unrelaxed	relaxed	unrelaxed	relaxed	unrelaxed
$\Delta z/\text{\AA}$	0.173	0.0	0.311	0.0	0.945	0.0
$S-M/\text{\AA}$	2.352	2.380	2.605	2.641	2.370	2.510
	3.008	2.906	3.334	3.168	3.420	3.035
$\Delta_{\text{bridge}}/\text{\AA}$	0.118	0.40	0.162	0.43	0.063	0.31
tilt/deg	53.8	52.1	54.5	49.8	62.7	56.4
$S-C/\text{\AA}$	1.853		1.847		1.844	

define the bridge site. The relaxation in the direction perpendicular to the surface (Δz) increases in the series Cu, Ag, Au, being considerably larger (nearly 1 Å) on the Au(111) surface. This leads to a strong decrease in the S–Au distance: it changes from 2.51 Å on the unrelaxed surface to 2.37 Å on the relaxed surface. The position of the sulfur atom on the surface becomes closer to the bridge site on all metals when the surface is allowed to relax. In the case of gold, the small value of Δ_{bridge} indicates that the sulfur atom is almost on the bridge site position, as can be seen in Figure 7c. On the other metals, the sulfur atom is shifted around 0.1 Å from the bridge site position in the direction of the fcc-hollow site. The relaxation of the metal atoms increases the tilt angle of the S–C bond with respect to the surface normal. This effect is more pronounced on gold: the tilt increases from 56.4° to 62.7°. The S–C bond length does not appreciably change between the relaxed and unrelaxed surfaces. In comparison, with the S–C bond length of 1.801 Å for the free adsorbate, we observe an enlargement of the bond length which is more important on the reactive copper surface (0.054 Å).

Adsorption under High Coverage. The high coverage regime was modeled using the slab approach for the ($\sqrt{3} \times \sqrt{3}$)R30° structure. Although other structures have been reported experimentally on Ag(111)²⁸ and Cu(111),²⁹ we used the same structure on all metals for comparison purposes. Figure 8 shows side and top views of the equilibrium structures. The adsorbate atoms and three of the four metal layers were relaxed in the optimizations. Binding energies were calculated for the relaxed and unrelaxed metal surfaces as shown in Table 5. The order of the binding energies is Cu > Ag > Au. The contribution of the metal relaxation to the binding energy is more important on gold than on the other metals. However, the contribution of the gold relaxation is smaller (−2.8 kcal/mol, Table 5) than in the low coverage limit (−10.63 kcal/mol, Table 3) indicating that the high thiol coverage inhibits the metal relaxation.

The structural parameters describing the relaxation of the adsorbate are shown in Table 6 for the relaxed and unrelaxed metal surfaces. Two of the three sulfur–metal bonds are shorter because the sulfur atom is near a bridge site as shown in Figure 8. The location of the sulfur atom above the surface is in an intermediate position between the hollow and bridge sites. Table 6 shows the horizontal displacement of the sulfur atom measured from the bridge (Δ_{bridge}) and hollow (Δ_{hollow}) sites. The sulfur atom is closer to the fcc-hollow site on Cu(111) and Ag(111), whereas it is closer to the bridge site on the Au(111) surface. The position of the sulfur atom above the surface varies considerably for the relaxed and unrelaxed metal surfaces. This points out the importance of considering the relaxation of the metal surface. From the comparison of Tables 3 and 5, it can be observed that the position of the sulfur atom above the surface is very sensitive to the surface coverage. In the low coverage limit, the bridge site is preferred on all metals, whereas under a high coverage, a position closer to the hollow site is obtained

**Figure 8.** Side and top views of equilibrium geometries of CH₃S adsorbed with a ($\sqrt{3} \times \sqrt{3}$)R30° structure on (a) Cu(111), (b) Ag(111), and (c) Au(111).**TABLE 5: Binding Energies (kcal/mol) of CH₃S Adsorbed with the ($\sqrt{3} \times \sqrt{3}$)R30° Structure on the Unrelaxed and Relaxed Metal Substrates^a**

	Cu		Ag		Au	
	BE	Δ BE	BE	Δ BE	BE	Δ BE
unrelaxed metal	−55.2		−45.3		−41.5	
relaxed metal	−56.1	−0.9	−47.1	−1.8	−44.3	−2.8

^a The three upper metal layers were relaxed.

TABLE 6: CH₃S Geometrical Parameters Calculated on the Relaxed and Unrelaxed Metal Surfaces for the ($\sqrt{3} \times \sqrt{3}$)R30° Structure

	Cu		Ag		Au	
	relaxed	unrelaxed	relaxed	unrelaxed	relaxed	unrelaxed
$S-M/\text{\AA}$	2.298	2.305	2.551	2.565	2.489	2.506
	2.302	2.314	2.553	2.574	2.494	2.579
	2.589	2.469	2.919	2.681	3.157	3.066
$\Delta_{\text{bridge}}/\text{\AA}$	0.554	0.582	0.627	0.737	0.393	0.278
$\Delta_{\text{hollow}}/\text{\AA}$	0.213	0.170	0.249	0.115	0.492	0.575
tilt/deg	36.12	33.78	44.86	39.85	50.8	51.00
$S-C/\text{\AA}$	1.847	1.848	1.839	1.843	1.832	1.837

for Cu and Ag and an intermediate position is observed on Au. The tilt angle of the S–C bond increases from copper to gold. The tilts obtained under high coverage (Table 6) are lower than

in the low coverage limit (Table 3) thus showing the effect of the surface coverage on the sulfur–metal bonding.

The relaxation of the metal surface can be appreciated in Figure 9. In the $(\sqrt{3} \times \sqrt{3})R30^\circ$ structure, there are three atoms in each layer of the unit cell and we considered the relaxation of the first three metal layers. Figure 9a shows the displacement from the equilibrium position in the xy plane parallel to the surface for each atom in each layer. Silver has the highest displacements followed by gold and copper. On the other hand, the highest relaxation along the direction perpendicular to the surface (Δz) is observed on gold as shown in Figure 9b. The average displacement of all the atoms in each layer is shown in parts c and d of Figure 9, respectively. These figures clearly show that the highest relaxation on the xy plane is observed for silver whereas gold has the highest relaxation along the direction perpendicular to the surface. Copper shows the smallest surface relaxation. In all cases, the surface relaxation decreases for the inner layers as expected.

Effect of Chain Length on the Potential Energy Surface on Au(111). The minima in Figure 2 have the S–C–H plane parallel to the plane normal to the surface. The potential energy of methanethiol increases when the S–C–H plane is tilted with respect to the surface normal. However, when we consider ethanethiol, we find two minima: one with the S–C–C plane normal to the surface and one with the S–C–C plane tilted with respect to the surface normal as shown in Figure 10. These two structures have comparable binding energies: -46.34 kcal/mol (Figure 10a) and -45.82 kcal/mol (Figure 10b). We found an equivalent structure for propanethiol on Cu(111)¹³ in which the tilted alkyl chain is oriented along one of the symmetry directions of the 111 surface. A major difference between the two structures in Figure 10 is the height of the carbon atom of the CH_3 group above the surface: 4.50 Å in Figure 10a and 3.80 Å in Figure 10b. The equilibrium tilt of the S–C–C plane with respect to the plane normal to the surface in Figure 10b is 52.0° . The structure in Figure 10b may not lead to a compact packing of the alkyl chains in a SAM, but it may likely occur at the boundary between ordered thiol domains.

Starting from the optimized structure of Figure 10b, which has the S–C–C plane tilted with respect to the surface normal, we calculated the potential energy as a function of the tilt of the molecular plane. At zero tilt, the plane of the molecule is perpendicular to the surface but it is rotated with respect to the normal plane which intersects the surface along the fcc-bridge-hcp direction (as is the case in Figure 10a). The lack of symmetry resulting from this rotation explains why the maximum energy in Figure 10c is not located at zero tilt. The potential energy surface shows a strong variation with the tilt of the molecular plane (an energy corrugation of around 10 kcal/mol) as expected for the more covalent sulfur–metal bonding on the Au(111) surface.

Electric Field Effects on the Potential Energy Surface. The adsorption mechanism of alkanethiols from aqueous solutions is electrochemical in nature because it involves electron-transfer steps. Alkanethiols adsorb on Au and Ag by an anodic oxidation reaction³⁰ which implies that the formation of the monolayer is facilitated at positive potentials. At negative enough potentials, on the other hand, the reductive desorption of the thiols occurs.³¹ These results indicate the importance of the electrode potential on the stability of SAMs of alkanethiols. Therefore, in this section, we considered the effect of the electric field on the potential energy surface of methanethiol on the three metals.

External uniform electric fields perpendicular to the surface in the range ± 0.01 au = $\pm 5.2 \times 10^7$ V/cm were considered.

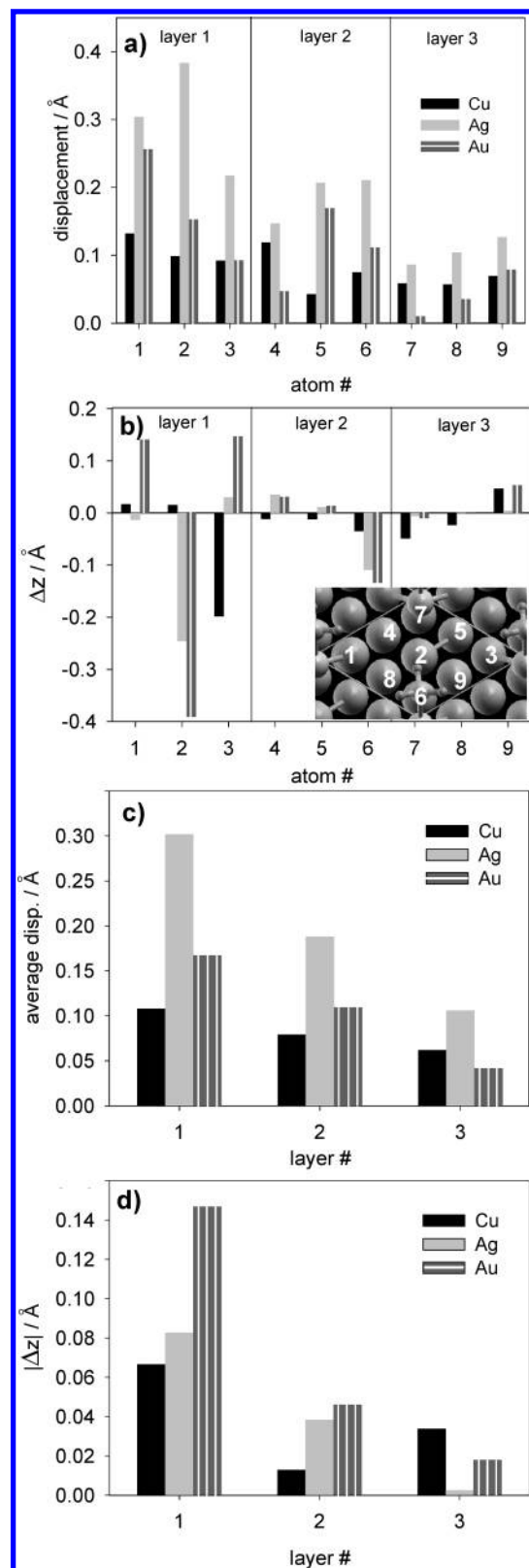


Figure 9. Relaxation of the atoms of the three upper surface metal layers: (a) displacement from the equilibrium position in the xy plane parallel to the surface, $(\Delta x^2 + \Delta y^2)^{1/2}$, (b) shift from the equilibrium position (Δz) in the direction perpendicular to the surface, (c) average displacement of the atoms in each layer in the xy plane, and (d) average shift from the equilibrium position of the atoms in each layer in the direction perpendicular to the surface, $(|\Delta z_1| + |\Delta z_2| + |\Delta z_3|)/3$.

These fields are comparable to those present in an electrochemical cell since an externally applied potential of 1 V creates an electric field of $\sim 10^7$ V/cm at the electrode surface.³² The

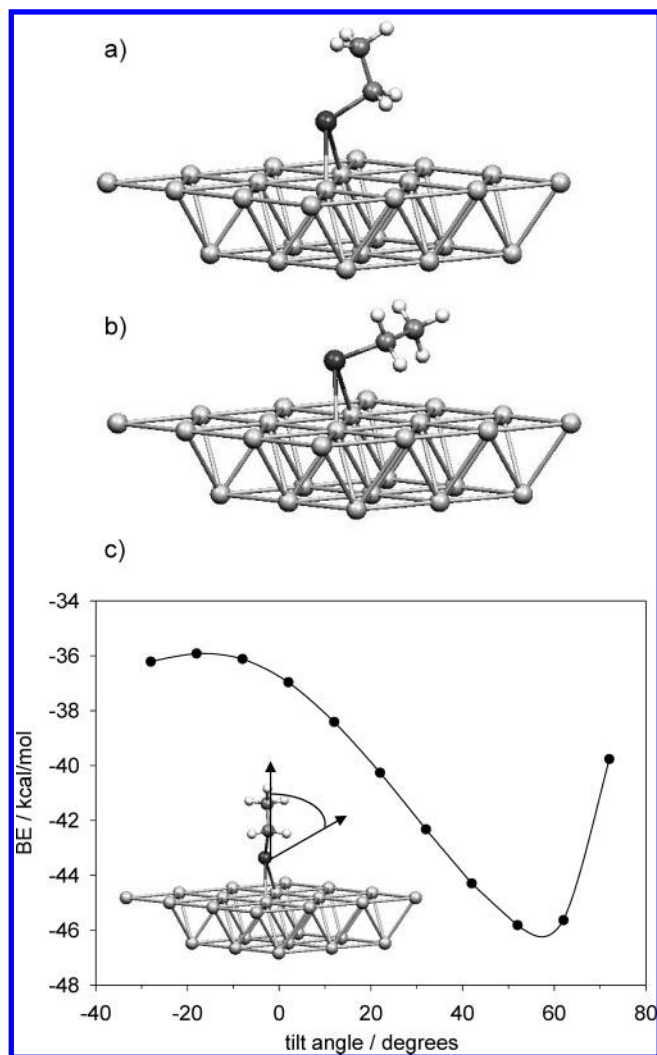


Figure 10. Two equilibrium structures of ethanethiol on Au(111): (a) S–C–C plane perpendicular to the surface, (b) tilted S–C–C plane, and (c) potential energy surface as a function of the tilt of the S–C–C plane.

TABLE 7: Binding Energies (kcal/mol) and S–M Bond Lengths (Å) of CH₃S Adsorbed on the fcc-bridge and ontop Sites as a Function of the Externally Applied Electric Field in a Direction Perpendicular to the Surface

site	<i>E</i> /au	Cu		Ag		Au	
		BE	S–Cu	BE	S–Ag	BE	S–Au
fcc-brd	–0.01	–43.23	2.47	–37.44	2.81	–35.60	2.62
	0.00	–48.20	2.38	–39.58	2.64	–42.36	2.51
	+0.01	–58.36	2.30	–47.21	2.56	–52.20	2.43
ontop	–0.01	–39.65	2.36	–35.06	2.64	–27.95	2.47
	0.00	–36.58	2.29	–28.23	2.54	–26.07	2.44
	+0.01	–38.22	2.26	–26.35	2.49	–29.56	2.42

calculations were performed using the cluster model of the surface keeping the metal atoms fixed. A positive field polarizes the electron density of the bare cluster leaving the surface layer with a depletion of electron density with respect to the zero field situation. The reverse trend is observed for negative fields.

Table 7 contains the CH₃S binding energies calculated on the fcc-bridge and ontop sites as a function of the electric field. The influence of the field on the binding energies and sulfur–metal bond lengths is more important on the fcc-bridge site than on the ontop site. This reflects the order of polarizability of the surface sites: the bridge site is the most polarizable whereas the ontop site is the least polarizable.³³ On the fcc-bridge site

TABLE 8: Corrugation of the Potential Energy Surface as a Function of the Electric Field^a

<i>E</i> /au	Cu	Ag	Au
–0.01	3.58	2.38	7.65
0.00	11.62	11.35	16.29
+0.01	20.14	20.86	22.64

^a The corrugation is defined as the difference in the CH₃S binding energies on the fcc-bridge and ontop sites.

of gold, for example, the change in binding energy between the negative and positive fields is 17 kcal/mol whereas the change in the S–Au bond length is 0.2 Å. On the ontop site, the corresponding changes in binding energy and S–Au bond length are only 3 kcal/mol and 0.05 Å, respectively. On the fcc-bridge site, the increase in binding energy with increasing field is accompanied by a decrease of the height of the sulfur atom above the surface and by a corresponding decrease of the sulfur–metal bond distance.

The energy difference between the most stable fcc-bridge and the least stable ontop sites defines the corrugation of the PES with respect to the adsorption site. Table 8 shows the corrugation of the PES as a function of the electric field. It can be observed that the electric field has an important influence on the PES: the surface corrugation decreases to a few kcal/mol at the negative field whereas it increases to more than 20 kcal/mol at the positive field. The corrugation on the Cu(111) and Ag(111) surfaces, on which the surface bonding is more ionic, shows a similar behavior. Higher corrugations are obtained on the Au(111) surface at all fields. This implies that the formation of a SAM is stabilized by positive potentials whereas the effect of negative potentials is to lower the barriers for surface diffusion. Therefore, the disordering of a SAM prior to the massive reductive desorption process will occur as a consequence of an increased surface mobility and higher S–Au bond lengths. These results show the advantage of forming SAMs under potential control as suggested by Paik et al.³⁰ The electrode potential must be considered as a tool to modify the corrugation of the PES. The changes in the PES corrugation with the electrode potential suggest that a SAM could undergo an electrochemical annealing process if the electrode potential is cycled between positive values in the stability region of the monolayer and negative values close to the reductive desorption potential.

Adsorption Site on Gold. In previous sections, we found that the methanethiol and ethanethiolate radicals adsorb on the perfect Au(111) surface on the fcc-bridge site in agreement with previous DFT calculations.⁴ However, two recent studies based on photoelectron diffraction³⁴ and normal incidence X-ray standing wave³⁵ techniques found that thiulates adsorb to singly coordinated sites on Au(111) instead of the bicoordinated bridge site found by DFT. This discrepancy could be due to different reasons: (a) the ontop adsorption site corresponds to a local minima not found yet in the potential energy surface under high coverage conditions, (b) DFT fails to adequately describe the surface bonding, (c) the surface modeling (alkanethiol radicals + perfect 111 surfaces) is oversimplified, and (d) chain–chain interactions influence the adsorption site. The first point will be considered in another work³⁶ in which we use the nudged elastic band method³⁷ to identify local minima and transition states in the potential energy surface. We do not think that DFT can fail to describe the strong surface bonds reported in this work. On the copper surface, for example, we found a very good agreement between the binding energy calculated at the DFT level and the one calculated at the HF + MP2 level.¹³ However, chain–chain interactions are not included in a DFT

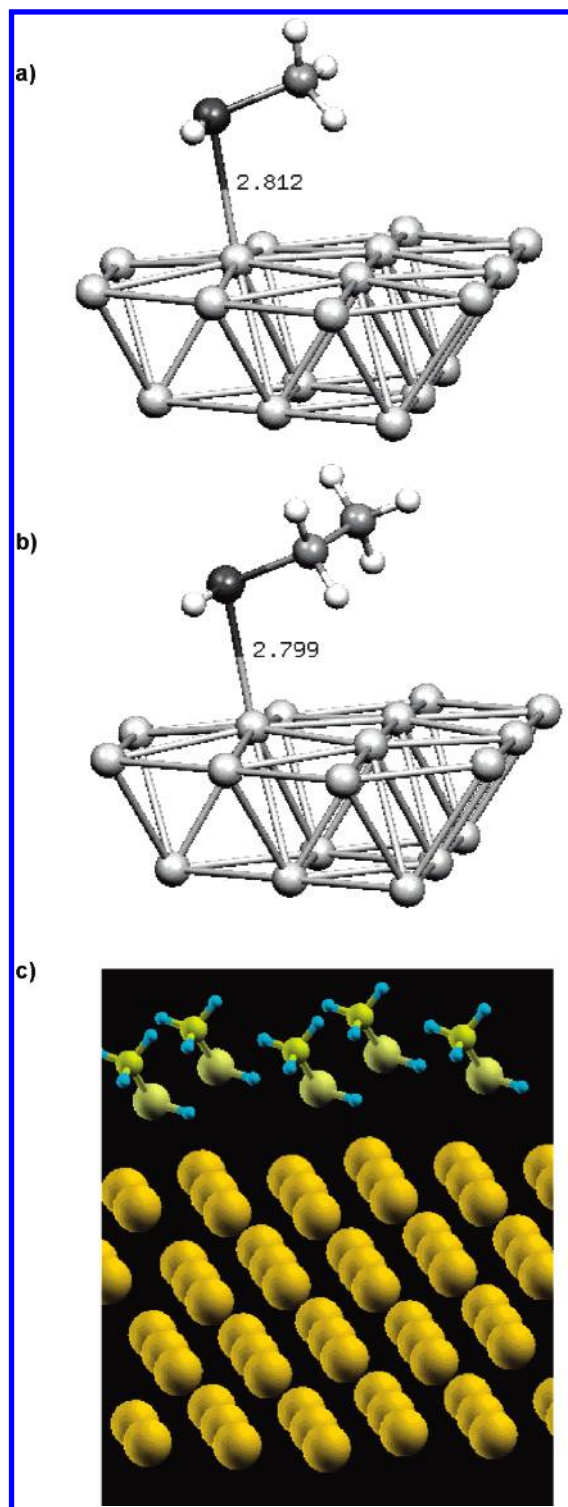


Figure 11. Molecular adsorption on Au(111) of (a) methanethiol and (b) ethanethiol in the low coverage limit. (c) Equilibrium geometry of the methanethiol molecule with the $(\sqrt{3} \times \sqrt{3})R30^\circ$ structure on Au(111).

calculation due to the well-known failure of DFT to describe dispersion forces.³⁸ In this section, we address point (c) considering different alternatives for the adsorbate and the metal surface: (i) adsorption of the molecular species on the perfect surface and (ii) adsorption of the radical species on a surface with a gold adatom. In the last case, we also investigate the diffusion of the thiol–Au moiety.

The adsorption of the molecular species occurs on the ontop site as shown in Figure 11 in the low and high coverage limits.

In the cluster calculations, the three central metal atoms were allowed to relax. The Au–S bond lengths of 2.812 Å (HSCH₃) and 2.799 Å (HSCH₂CH₃) are higher than the values in the range of 2.40–2.50 Å obtained for the chemisorbed species (see Table 4). The molecular adsorption geometry in Figure 11 shows that the nonbonding orbitals around the S atom are involved in the interaction with the metal surface. Although the binding energies are small, –10.1 kcal/mol for HSCH₃ and –11.1 kcal/mol for HSCH₂CH₃, the molecular adsorption induces an upward relaxation (0.35 Å) of the gold atom closer to the sulfur atom. Under high coverage conditions, HSCH₃ also adsorbs via the sulfur atom on an ontop position, although the Au–S distance is longer, 3.29 Å, and the binding energy, –4.09 kcal/mol, is lower than in the low coverage limit. These S–Au bond lengths are larger than the experimental values in the range of 2.40–2.50 Å.^{34,35} Therefore, the ontop adsorption on gold cannot be ascribed to the presence of a molecular species. However, this seems to occur on the Ag(110) surface on which the nondissociative chemisorption of methanethiol has been reported.³⁹ Perhaps the initial ontop adsorption of the molecular species somehow affects the packing of the alkyl chains during the formation of a SAM thus leading to an ontop adsorption of the radical species after the cleavage of the S–H bond. Whether a small fraction of thiols may remain in a molecular form on the surface with the corresponding influence on the SAM packing is an open question.

The adsorption of ethanethiol in the presence of a gold adatom on the Au(111) surface occurs ontop of the surface adatom as shown in Figure 12a. We considered the ethanethiolate radical to take into account any possible chain length effects. The surface metal atoms were kept fixed whereas the geometry of CH₃CH₂SAu was optimized. The most stable structure was found when the gold atom bound to ethanethiol was on the hcp site. The Au–S distance of 2.30 Å is shorter than that of ethanethiol adsorbed on the perfect surface (2.50 Å, Figure 10) indicating a stronger bonding. The binding energy of ethanethiol on the Au(111)/Au surface is –67.6 kcal/mol whereas on the perfect Au(111) surface (Figure 10a) the binding energy is –46.3 kcal/mol.

We next optimized the structure of CH₃CH₂SAu on the fcc and bridge sites. On the bridge site, the Au atom of the CH₃CH₂SAu moiety was constrained to be on the bridge position: only the coordinate perpendicular to the surface was allowed to relax, whereas all the coordinates of the other atoms were relaxed. In all cases, the sulfur atom is located ontop of the gold adatom. Figure 12b shows the relative energies obtained on the different sites taking as a reference the most stable hcp site. Both hollow sites are nearly isoenergetic. The activation barriers for diffusion are very small: 1.64 kcal/mol (fcc → hcp) and 2.24 kcal/mol (hcp → fcc). These barriers are smaller than the barriers for the diffusion of a single gold atom on Au(111) as shown in Figure 12b. This is due to the weakening of the Au–Au bonds as a consequence of the formation of a strong S–Au bond (around 20 kcal/mol more stable than on the perfect surface) between ethanethiol and the gold adatom. The diffusion of the thiol–Au moiety also has considerably smaller barriers than those for the diffusion of a bare thiol. As shown in Figure 2, the diffusion of methanethiol from the fcc to the hcp-hollow sites has an energy barrier of 17.6 kcal/mol. Therefore, alkanethiols increase the mobility of gold atoms at the surface. These results suggest that the formation of a monolayer may involve the diffusion and self-assembly of thiolate–Au moieties rather than the diffusion of the bare thiolates across the surface.

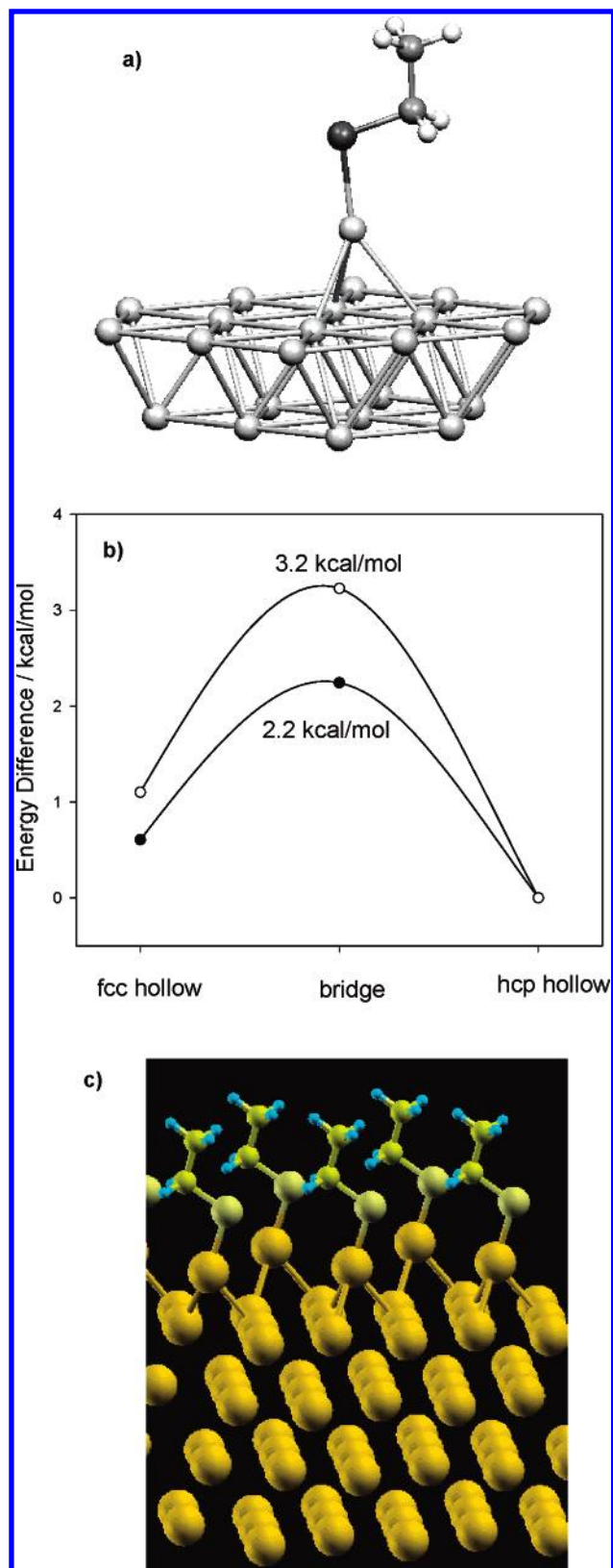


Figure 12. (a) Equilibrium structure of ethanethiol adsorbed on a surface adatom on Au(111). The most stable surface site is the hcp-hollow site. (b) Potential energy calculated for the bare Au adatom and for ethanethiol adsorbed on the adatom as a function of the surface site. (c) Equilibrium geometry of CH₃CH₂SAu with a $(\sqrt{3} \times \sqrt{3})R30^\circ$ structure.

The diffusion of thiol–Au moieties may be the driving force leading to the formation of a defected layer of gold atoms below the thiol monolayer. If every thiolate drags a gold atom during

the self-assembly process, for example, a defected gold layer with a surface coverage of 0.33 can be formed. The formation of a defected layer of gold atoms below the thiol monolayer is compatible with the enhanced surface mobility of gold atoms induced by the adsorption and desorption of thiols. The adsorption of thiols is characterized by the appearance of vacancy islands and the lifting of gold reconstruction whereas during the reductive desorption process, the roughening of step edges, and the appearance of gold islands has been observed.^{40,41}

The ontop adsorption on gold adatoms is also stable under high coverage. The equilibrium geometry of CH₃CH₂SAu on Au(111) with a $(\sqrt{3} \times \sqrt{3})R30^\circ$ structure is shown in Figure 12c. The S–Au bond length (2.29 Å) is shorter than for adsorption on the perfect Au(111) surface (2.49 Å) indicating a stronger surface bonding on the defected gold layer. The ethanethiol binding energy on this layer is –56.0 kcal/mol whereas on the perfect Au(111) surface the binding energy is –44.3 kcal/mol. The structure in Figure 12c has the S–C–C plane perpendicular to the surface. We also found a nearly isoenergetic structure with the molecular plane tilted as shown in Figure 10 for ethanethiol. Therefore, adsorption on a defected layer of gold atoms may be a possible explanation for the experimentally observed ontop site adsorption. The ontop adsorption site has also been reported for methanethiol adsorbed on a defected gold layer in which two gold atoms are missing for every three.⁹

Conclusions

The adsorption of alkanethiols was studied comparatively on Cu(111), Ag(111), and Au(111) surfaces under low and high coverages in the absence and presence of external electric fields. In the low coverage limit, qualitatively similar adsorption structures were obtained on the three metals: the most stable adsorption site for the methanethiolate radical is the bridge site slightly off-centered toward the fcc site with the S–C bond tilted between 50° and 60° with respect to the surface normal. However, under high coverage, the sulfur atom is closer to the fcc-hollow site on Cu(111) and Ag(111), whereas it is closer to the bridge site on Au(111). The ontop site is the least stable for all metals. For alkanethiols with longer chains, the potential energy surface has another minimum in which the molecular plane is tilted with respect to the surface. The effect of the tilt of the S–C bond on the binding energy is more pronounced on the Au(111) surface, due to a higher covalent contribution to the bonding than on the Ag(111) and Cu(111) surfaces. The high corrugation of the PES on gold with the tilt angle implies that the interconversion among different rotational domains will have high activation energies.

The effect of the substrate relaxation was considered under high and low coverages. The contribution of the surface relaxation to the adsorbate binding energy is more important on gold than on the other metals. The relaxation of gold is higher in the low coverage limit, and it mainly consists of an upward movement of the metal atoms. On the silver surface, we observed the highest relaxation in a plane parallel to the surface. When the metal substrate is kept fixed in the low coverage limit, the order of the CH₃S• binding energies is Cu > Ag > Au. However, when the surface-relaxation contribution to the binding energy is taken into account, the order of the binding energies becomes Cu > Au > Ag. In the $(\sqrt{3} \times \sqrt{3})R30^\circ$ structure, the order of the binding energies is Cu > Ag > Au.

External electric fields applied in a direction perpendicular to the surface were employed to simulate the effect of the electrode potential. The electric field has an important effect

on the corrugation of the potential energy surface. The corrugation increases (decreases) at positive (negative) fields. The decrease in surface corrugation at a negative field is more pronounced on Cu and Ag on which the bonding is more ionic. Gold has higher corrugations at all fields. Therefore, the cycling of the electrode potential between positive and negative values could be used to induce an electrochemical annealing in a SAM.

The adsorption site on gold was also investigated for a molecular species as well as on defected surfaces. The sulfur atom adsorbs on the ontop site for the CH_3SH and $\text{CH}_3\text{CH}_2\text{SH}$ species. The corresponding radicals only adsorb on ontop sites when gold adatoms are on the surface. The diffusion of the $\text{CH}_3\text{CH}_2\text{SAu}$ species has a lower barrier than the diffusion of a bare gold atom and a bare thiol radical, indicating that the formation of a monolayer may involve the diffusion and self-assembly of thiolate–Au moieties rather than the diffusion of the bare thiolates across the surface.

Acknowledgment. E.M.P. thanks Fundación Antorchas for Grant A-13532/1-102. P.P.O. thanks grants from CONICET and Fundación Antorchas. We also thank the support of Agencia Nacional de Promoción Científica y Tecnológica (Grant No. 06-03195), Agencia Córdoba Ciencia, and SECYT-UNC. F.P.C. thanks CONICET for the fellowships granted.

References and Notes

- (1) Sellers, H.; Ulman, A.; Shnidman, Y.; Eilers, J. E. *J. Am. Chem. Soc.* **1993**, *115*, 9389.
- (2) Grönbeck, H.; Curioni, A.; Andreoni, W. *J. Am. Chem. Soc.* **2000**, *122*, 2839.
- (3) Vargas, M. C.; Giannozzi, P.; Selloni, A.; Scoles, G. *J. Chem. Phys.* **2001**, *105*, 9509.
- (4) Hayashi, T.; Morikawa, Y.; Nozoye, H. *J. Chem. Phys.* **2001**, *114*, 7615.
- (5) Akinaga, Y.; Nakakima, T.; Hirao, K. *J. Chem. Phys.* **2001**, *114*, 8555.
- (6) Gottschalk, J.; Hammer, B. *J. Chem. Phys.* **2002**, *116*, 784.
- (7) Yourdshahyan, Y.; Rappe, A. M. *J. Chem. Phys.* **2002**, *117*, 825.
- (8) Morikawa, Y.; Liew, C. C.; Nozoye, H. *Surf. Sci.* **2002**, *514*, 389.
- (9) Molina, L.; Hammer, B. *Chem. Phys. Lett.* **2002**, *360*, 264.
- (10) Franzen, S. *Chem. Phys. Lett.* **2003**, *381*, 315.
- (11) Cao, Y.; Ge, Q.; Dyer, D.; Wang, L. *J. Phys. Chem. B* **2003**, *107*, 3803.
- (12) De Renzi, V.; Di Felice, R.; Marchetto, D.; Biagi, R.; Del Pennino, U.; Selloni, A. *J. Phys. Chem. B* **2004**, *108*, 16.
- (13) Ferral, A.; Paredes-Olivera, P.; Macagno, V. A.; Patrito, E. M. *Surf. Sci.* **2003**, *525*, 85.
- (14) Patrito, E. M.; Cometto, F. P.; Paredes-Olivera, P. *J. Phys. Chem. B* **2004**, *108*, 15755.
- (15) Vosko, S. H.; Wilk, L.; Nusair, M. *Can. J. Phys.* **1980**, *58*, 1200.
- (16) Becke, A. D. *Phys. Rev. A* **1988**, *38*, 3098.
- (17) Perdew, J. P.; Wang, Y. *Phys. Rev. B* **1992**, *45*, 13244.
- (18) Lee, C.; Yang, W.; Parr, R. G. *Phys. Rev. B* **1988**, *37*, 785.
- (19) Perdew, J. P.; Burke, K.; Wang, Y. *Phys. Rev. B* **1996**, *54*, 16533.
- (20) van Lenthe, E.; Ehlers, A. E.; Baerends, E. J. *J. Chem. Phys.* **1999**, *110*, 8943.
- (21) Baerends, E. J.; Bérces, A.; Bo, C.; Boerrigter, P. M.; Cavallo, L.; Deng, L.; Dickson, R. M.; Ellis, D. E.; Fan, L.; Fischer, T. H.; Fonseca Guerra, C.; van Gisbergen, S. J. A.; Groeneveld, J. A.; Gritsenko, O. V.; Harris, F. E.; van den Hoek, P.; Jacobsen, H.; van Kessel, G.; Kootstra, F.; van Lenthe, E.; Osinga, V. P.; Philipsen, P. H. T.; Post, D.; Pye, C. C.; Ravenek, W.; Ros, P.; Schipper, P. R. T.; Schreckenbach, G.; Snijders, J. G.; Sola, M.; Swerhone, D.; te Velde, G.; Vernooijs, P.; Versluis, L.; Visser, O.; van Wezenbeek, E.; Wiesenekker, G.; Wolff, S. K.; Woo, T. K.; Ziegler, T.; Fonseca Guerra, C.; Snijders, J. G.; te Velde, G.; Baerends, E. J. *Theor. Chem. Acc.* **1998**, *99*, 391.
- (22) Baroni, S.; Dal Corso, A.; De Gironcoli, S.; Giannozzi, P. <http://www.pwscf.org>.
- (23) Perdew, J. P.; Burke, K.; Ernzerhof, M. *Phys. Rev. Lett.* **1996**, *77*, 3865.
- (24) Vanderbilt, D. *Phys. Rev. B* **1990**, *41*, 7892.
- (25) Monkhorst, H. J.; Pack, J. D. *Phys. Rev. B* **1976**, *13*, 5188.
- (26) van den Hoek, P. J.; Baerends, E. J.; van Santen, R. A. *J. Phys. Chem.* **1989**, *93*, 6469.
- (27) Shustorovich, E.; Sellers, H. *Surf. Sci. Rep.* **1998**, *31*, 1.
- (28) Kawasaki, M.; Nagashima, H. *Surf. Sci.* **2004**, *549*, 237.
- (29) Driver, S. M.; Woodruff, D. P. *Langmuir* **2000**, *16*, 6693.
- (30) Paik, W.-K.; Eu, S.; Lee, K.; Chon, S.; Kim, M. *Langmuir* **2000**, *16*, 10198.
- (31) Porter, M. D.; Bright, T. B.; Allara, D. L.; Chidsey, Ch. E. D. *J. Am. Chem. Soc.* **1987**, *109*, 3559.
- (32) Nart, F. C.; Iwasita, T. *Electrochim. Acta* **1996**, *41*, 631.
- (33) Pacchioni, G. *Electrochim. Acta* **1996**, *41*, 2285.
- (34) Kondoh, H.; Iwasaki, M.; Shimada, T.; Amemiya, K.; Yokoyama, T.; Ohta, T.; Shimomura, M.; Kono, S. *Phys. Rev. Lett.* **2003**, *90*, 066102.
- (35) Roper, M. G.; Skegg, M. P.; Fisher, C. J.; Lee, J. J.; Dhanak, V. R.; Woodruff, D. P.; Jones, R. G. *Chem. Phys. Lett.* **2004**, *389*, 87.
- (36) Patrito, E. M.; Cometto, F. P.; Macagno, V. A.; Paredes-Olivera, P. In preparation.
- (37) Henkelman, G.; Uberuaga, B. P.; Jonsson, H. *J. Chem. Phys.* **2000**, *113*, 9901.
- (38) Kristyán, S.; Pulay, P. *Chem. Phys. Lett.* **1994**, *229*, 175.
- (39) Lee, J. G.; Lee, J.; Yates, J. T. *J. Am. Chem. Soc.* **2004**, *126*, 440.
- (40) Wano, H.; Uosaki, K. *Langmuir* **2001**, *17*, 8224.
- (41) Carot, M. L.; Esplandiu, M. J.; Cometto, F. P.; Patrito, E. M.; Macagno, V. A. *J. Electroanal. Chem.* **2005**, *579*, 13.